Advances in Materials and Processing Technologies

A parametric numerical study of ASB-assisted chip formation in high-speed machining of Ti-6Al-4V

--Manuscript Draft--

Full Title:	A parametric numerical study of ASB-assisted chip formation in high-speed machining of Ti-6Al-4V
Manuscript Number:	TMPT-2019-0041R1
Article Type:	Research Article
Keywords:	High-speed machining; thermomechanical coupling; inelastic heat fraction; critical strain; viscoplasticity
Abstract:	The present study aims at studying the influence of some parameters on the numerical results obtained from the simulation of the high-speed machining process using a commercial finite element computation code, namely Abaqus-Exp. Starting from models available by default in the computation code, comparisons are made between full and weak thermomechanical coupling, and the influence of the fracture strain and inelastic heat fraction values are studied. The high-strength Ti-6Al-4V titanium alloy is taken as example. Continuous, serrated and segmented chips are reproduced at low, moderate and high cutting speeds and the differences observed between experimental and numerical results are discussed.
Order of Authors:	Hannah Lois-Dorothy
	Xavier Soldani
	Patrice Longère
Response to Reviewers:	Please see attached file

A parametric numerical study of ASB-assisted chip formation in high-speed machining of Ti-6Al-4V

Hannah Lois Dorothy[a], Xavier Soldani[b], Patrice Longère[c1]

[a] Expleo Group, Toulouse, France, hannah.anandan@expleogroup.com

[b] Universidad Pontificia Comillas ICAI-ICADE, Madrid, Spain, xsoldani@icai.comillas.edu

[c] Institut Clément Ader, Université de Toulouse, ISAE-SUPAERO, UT3/UPS, INSA-T, IMT Mines Albi, CNRS, Toulouse, France, patrice.longere@isae.fr

Keywords: High-speed machining, thermomechanical coupling, inelastic heat fraction, critical strain, viscoplasticity.

Abstract. The present study aims at studying the influence of some parameters on the numerical results obtained from the simulation of the high-speed machining process using a commercial finite element computation code, namely Abaqus-Exp. Starting from models available by default in the computation code, comparisons are made between full and weak thermo-mechanical coupling, and the influence of the fracture strain and inelastic heat fraction values are studied. The high-strength Ti-6Al-4V titanium alloy is taken as example. Continuous, serrated and segmented chips are reproduced at low, moderate and high cutting speeds and the differences observed between experimental and numerical results are discussed.

1. Introduction

Thanks to its versatility, reliability and relatively low cost, machining still remains widely used for manufacturing metal pieces. In the aim of improving the process productivity, an increase in the cutting speed is notably sought. This increase in the cutting speed has a strong influence on the tool-chip-workpiece interactions with potentially new issues and unwished consequences, as for example a premature degradation of the tool material implying thus specific coating, see e.g. see Hemmati et al. (2022) and Chowdhury et al. (2020). Depending on the material properties (composition, strength, ductility, etc), the chip formation may strongly depend on the removal rate with continuous, serrated and segmented chips observed at low, moderate and high cutting speeds, respectively, see e.g. Moufki et al. (2004) and Ye et al. (2013). As expected, this evolution of the chip morphology is accompanied by changes in the workpiece surface roughness quality, hence the need for optimizing the high-speed

[1] Corresponding author: patrice.longere@isae.fr

machining conditions. A better understanding and modeling of the thermo-mechanical couplings operating during the machining process is thus required.

In this context, several experimental studies have been dedicated to reproducing the high-speed machining conditions, generally by either using a small gas gun or adapting the split Hopkinson pressure bar set-up, see e.g. Sutter et al. (1998), Gente and Hoffmeister (2001), Molinari et al. (2002) and Larbi et al. (2015). Some machining operations were also equipped with high-speed infrared camera, see e.g. Ivester et al. (2005) and Abukshim et al. (2006). Some attempts of describing the machining process have been made following analytical approaches, see e.g. Moufki et al (1998) and Chen et al. (2021), bringing some highlights and trends but too limited to specific machining configurations to be generalized and applicable to complex processes. For this reason, numerical simulations are widely used employing mostly the finite element method (FEM), see e.g. Umbrello (2008), and sometimes particle-based methods, like smooth particle hydrodynamics (SPH), see e.g. Xi et al. (2014).

During high-speed cutting, the rate of deformation of the workpiece material may locally reach values of the order of 10^3 s^{-1}. Moreover, in metal machining in general and high-speed metal machining in particular, friction and plastic dissipation are known to play a major role as sources of local heating, with temperatures approaching and even attaining the melting point, see Abukshim et al. (2006). A constitutive model able to reproduce the material response all along the machining process is thus expected to be rate- and temperature-dependent, see a recent review on behavior laws applied to machining in Melkote et al. (2017). The constitutive model must be completed by a failure criterion that, depending on the material ductility, results from continuum damage mechanics (CDM), see examples in Lemaître (1985) and Longère and Dragon (2013), or merely from a (more or less multi-dependent) strain-controlled fracture indicator, see examples in Johnson and Cook (1985) and Bao and Wiezbicki (2004). It is noteworthy that some commercial computation codes proposed mixed indicator-CDM models for damage initiation and evolution, see e.g. an application to high-speed machining in Mabrouki et al. (2008). There is a phenomenon called adiabatic shear banding (ASB) that specifically occurs under high strain rate loading in the form of narrow bands as the result of the competition operating inside the material between strain and strain rate hardening on the one side and thermal softening on the other side, see Bai and Dodd (1992). ASB may be considered as a premature failure mechanism in the sense that it locally softens the material resistance and is precisely the mechanism that favors the chip serration and segmentation observed in high strength metals and alloys. Yet, in spite of its major role in dynamic plasticity, ASB is rarely explicitly accounted for in numerical simulations, see however some approaches

in Longère et al. (2009) and Dorothy and Longère (2019) as well as a review in Longère (2018) on the issues related to ASB modeling. One can also quote the physics-motivated constitutive models aimed at reproducing the microstructural changes involved during high-speed machining, see e.g. Liu et al. (2020), Xu et al. (2020) and Fu et al. (2021). At last, in numerical simulations, the thermo-mechanical couplings may be fully or weakly accounted for. In the former both heat and mechanical equilibrium equations are solved, taken thermal diffusion into account if needed, whereas in the latter the sole mechanical equilibrium equation is solved, under the hypothesis of adiabatic conditions.

In view of evidencing some issues/limitations in the numerical simulation of high-speed machining and providing the designer with elements for parameterizing his/her optimization process, the present engineering-oriented study focuses on the influence of the way the thermo-mechanical coupling and material failure are accounted for. More precisely, starting from models available by default in the computation code, comparisons will be made between full and weak thermo-mechanical coupling, and the influence of the fracture strain and inelastic heat fraction values will be studied. As a high-strength material widely used in aerospace engineering, difficult to machine and particularly susceptible to ASB due to its low thermal conductivity, the high-strength Ti-6Al-4V titanium alloy is here taken as example with most of the above quoted works referring to. The numerical simulations are conducted employing the commercial finite element computation code Abaqus-Exp.

Section 2 presents the constitutive model and thermal considerations. The high-speed machining numerical procedure is outlined in Section 3. Numerical simulations and results are shown and commented in Section 4. In Section 5, numerical simulations are discussed and some recommendations are suggested. Finally, conclusions are drawn in Section 6.

2. Constitutive model and thermal considerations

The main considerations related to the constitutive modeling and thermal hypotheses are presented in this section.

- *Yield function*

In temperature-dependent viscoplasticity, the yield function f may be written as

$$f\left(\underline{\underline{\sigma}},\sigma_y\right)=\sigma_{eq}\left(\underline{\underline{\sigma}}\right)-\sigma_y\left(\varepsilon_p,T\right)=\sigma_v\left(\varepsilon_p,\dot{\varepsilon}_p,T\right)\geq 0 \tag{1}$$

where σ_{eq} is the Mises equivalent stress, $\sigma_{eq}\left(\underline{\underline{\sigma}}\right)=\sqrt{\frac{3}{2}\underline{\underline{s}}:\underline{\underline{s}}}$, with $\underline{\underline{\sigma}}$ the Cauchy stress and $\underline{\underline{s}}$ its deviatoric part, $\underline{\underline{s}}=\underline{\underline{\sigma}}-\frac{Tr\underline{\underline{\sigma}}}{3}\underline{\underline{I}}$, $\underline{\underline{I}}$ the identity tensor; σ_y and σ_v represent the rate-independent yield stress and rate-dependent overstress or viscous stress, respectively; ε_p and $\dot{\varepsilon}_p$ are the cumulated plastic strain and strain rate and *T* the temperature.

Equation (1) yields

$$\sigma_{eq}\left(\underline{\underline{\sigma}}\right)=\sigma_y\left(\varepsilon_p,T\right)+\sigma_v\left(\varepsilon_p,\dot{\varepsilon}_p,T\right)=\bar{\sigma}_y\left(\varepsilon_p,\dot{\varepsilon}_p,T\right) \tag{2}$$

where $\bar{\sigma}_y$ represents the rate- and temperature-dependent yield stress.

The (intrinsic) plastic dissipation *D* may be expressed in the form

$$D=\beta\dot{W}_p\geq 0\,;\dot{W}_p=\underline{\underline{\sigma}}:\underline{\underline{\dot{\varepsilon}}}_p \tag{3}$$

where $\dot{W}_p$ represents the plastic work rate and $\underline{\underline{\dot{\varepsilon}}}_p$ the instantaneous plastic strain rate obeying the normality rule:

$$\underline{\underline{\dot{\varepsilon}}}_p=\dot{\varepsilon}_p\frac{\partial f}{\partial\underline{\underline{\sigma}}}=\frac{3}{2}\dot{\varepsilon}_p\frac{\underline{\underline{s}}}{\sigma_{eq}} \tag{4}$$

The quantity β in (3) represents the proportion of plastic work rate $\dot{W}_p$ dissipated.

Equations (2) and (4) yields

$$\dot{\varepsilon}_p=\sqrt{\frac{2}{3}\underline{\underline{\dot{\varepsilon}}}_p:\underline{\underline{\dot{\varepsilon}}}_p}\geq 0\ ;\ \varepsilon_p=\int_t\dot{\varepsilon}_p dt\geq 0\ ;\ \dot{W}_p=\sigma_{eq}\dot{\varepsilon}_p=\bar{\sigma}_y\dot{\varepsilon}_p \tag{5}$$

- *Johnson-Cook constitutive model*

Due to its engineering-oriented formulation, the Johnson-Cook model, see Johnson and Cook (1983), and its numerous variants are widely used to describe the workpiece material behavior during HSM, see e.g. Seo et al. (2005), Calamaz et al. (2008), Wang et al. (2015), Zhang et al.

(2015) as well as some already cited papers. The Johnson-Cook rate- and temperature-dependent yield stress includes a multiplicative contribution of the combined effects of strain hardening, strain rate hardening and thermal softening:

$$\bar{\sigma}_y\left(\varepsilon_p,\dot{\varepsilon}_p,T\right)=(A+B\varepsilon_p^n)\left(1+C\ln\frac{\dot{\varepsilon}_p}{\dot{\varepsilon}_0}\right)\left(1-\left(\frac{T-T_0}{T_m-T_0}\right)^m\right) \tag{6}$$

where $\dot{\varepsilon}_0$ is a reference strain rate, T_0 a reference temperature and T_m the melting temperature; A,B,n,m are constants.

By combining (2) and (6), one has

$$\begin{cases}\sigma_y\left(\varepsilon_p,T\right)=(A+B\varepsilon_p^n)\left(1-\left(\frac{T-T_0}{T_m-T_0}\right)^m\right)\\ \sigma_v\left(\varepsilon_p,\dot{\varepsilon}_p,T\right)=(A+B\varepsilon_p^n)C\ln\frac{\dot{\varepsilon}_p}{\dot{\varepsilon}_0}\left(1-\left(\frac{T-T_0}{T_m-T_0}\right)^m\right)\end{cases} \tag{7}$$

According to (7), the Johnson-Cook model assumes that both rate-independent yield stress and viscous stress depend on strain, strain rate and temperature.

- *Thermal considerations*

The local form of the heat equation reads

$$\rho C_p\dot{T}-k\Delta T=\dot{Q} \tag{8}$$

where $\dot{T}$ is the heating rate and ΔT is the Laplacian of T; ρ, C_p and k represent the mass density, the specific heat and the thermal conductivity, respectively; $\dot{Q}$ is the heat source.

Under certain hypotheses, see Longère and Dragon (2008, 2009), the heat source $\dot{Q}$ reduces to the plastic dissipation D, viz. $\dot{Q}=D$. The coefficient β is thus the Taylor-Quinney inelastic heat fraction, see Taylor and Quinney (1934), and the heat equation in (8) becomes

$$\rho C_p \dot{T} - k\Delta T = \beta \bar{\sigma}_y \dot{\varepsilon}_p \tag{9}$$

Under adiabatic conditions, (9) finally reduces to

$$\rho C_p \dot{T} = \beta \bar{\sigma}_y \dot{\varepsilon}_p \tag{10}$$

According to (9-10), the inelastic heat fraction β controls the temperature rise and then the thermal softening potentially triggering ASB. While it has been shown to be strain and strain rate dependent from both experimental and theoretical perspectives, see e.g. Mason et al. (1994) Rosakis et al. (2000), and Longère and Dragon (2008, 2009), the inelastic heat fraction is generally considered as constant with values comprised between 0.8 and 1, meaning that 80 to 100% of the plastic work rate $\dot{W}_p$ are dissipated as heat.

- *Failure criterion*

The Ti-6Al-4V titanium alloy ductility strongly depends on its thermo-mechanical history (heat-treatment, cold-rolling, forging, etc). The ductility is here associated with the amount of plastic strain between micro-voiding initiation (which is delayed with respect to plastic strain occurrence) and full fracture during the damage-induced drop in resistance. This amount is a more or less important part of the overall plastic strain at fracture. As mentioned in the Introduction, depending on the material ductility, the ultimate material failure may be reproduced by either applying the CDM concepts (high ductility involving a progressive drop in resistance) or using a mere strain-controlled fracture criterion (low ductility involving a relatively brutal drop in resistance). According to Ruiz de Sotto et al. (2021), we consider here a low ductility Ti-6Al-4V titanium alloy grade and accordingly use a fracture criterion. There exist many strain-controlled fracture criteria accounting for strain rate, temperature, stress triaxiality ratio and/or Lode parameter, see e.g. Wang and Liu (2016). There is no universal strain-controlled fracture criterion, even for Ti-6Al-4V titanium alloys, see Ruiz de Sotto et al. (2021), and in this context we consider a fracture criterion that depends on the sole plastic strain written in terms of critical plastic strain denoted ε_p^{crit}.

As soon as $\varepsilon_p = \varepsilon_p^{crit}$, the failure of the material results numerically in the finite element deletion (total loss of resistance with mass conservation).

- *Friction at the work piece/tool interface*

Although the heat generated due to friction is not considered in the present parametric study, the mechanical contact at the tool-chip interface is simulated with the Coulomb friction law.

3. Numerical procedure

Numerical simulations are conducted with the commercial computation code Abaqus using the explicit time integration scheme and the finite element space discretization.

For the weak thermo-mechanical coupling, adiabatic conditions are assumed and the heating rate $\dot{T}$ is accordingly governed by (10).

For the full thermo-mechanical coupling, the heating rate $\dot{T}$ is governed by (9). As mentioned in Abaqus documentation, in most applications of explicit analysis the mechanical response controls the stability. The maximum stable time increment size Δt is accordingly

$$\Delta t \le \min\left[\Delta t_T ; \Delta t_M\right] ; \Delta t_T = \frac{\ell_{min}^2}{2\alpha} ; \Delta t_M = \frac{\ell_{min}}{c_{max}} ; \alpha = \frac{k}{\rho C_p} ; c = \sqrt{\frac{\lambda+\mu}{\rho}} \tag{11}$$

where Δt_T and Δt_M are the stable time increment sizes for the thermal and mechanical analyses, respectively; ℓ_{min} is the smallest finite element dimension, c is the dilatational wave speed and (λ,μ) are Lamé elastic constants, μ is the shear modulus.

- Geometry

The geometry for the high-speed orthogonal cutting simulated set-up is inspired from Molinari et al. (2013), see Fig.1a. The important feature to note in this geometry is that the workpiece is divided into three different parts: zone A which forms the chip, zone B is the intermediate layer and zone C is the workpiece base. The workpiece total width and thickness are 2mm and 500µm, respectively, and zones A and B have the same thickness of 100µm. The feed t_1 is accordingly 100µm. The tool rake and clearance angles are 0 and 7°, respectively, and the tool radius is 16µm.

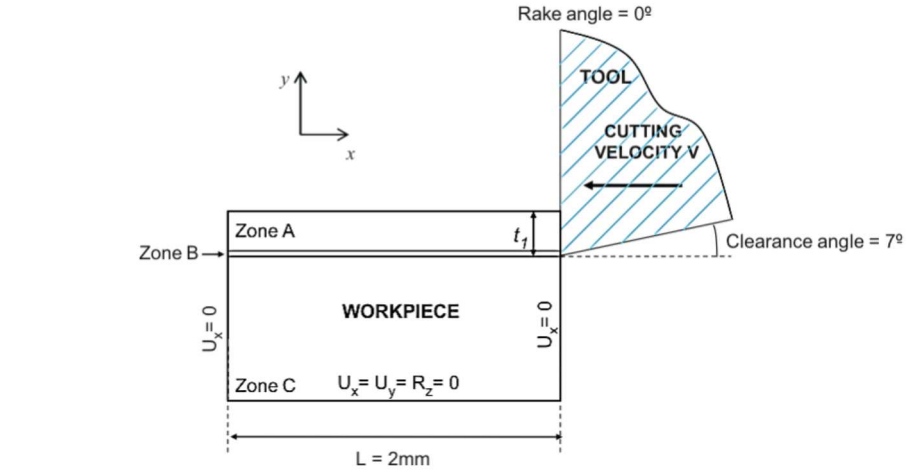

a)

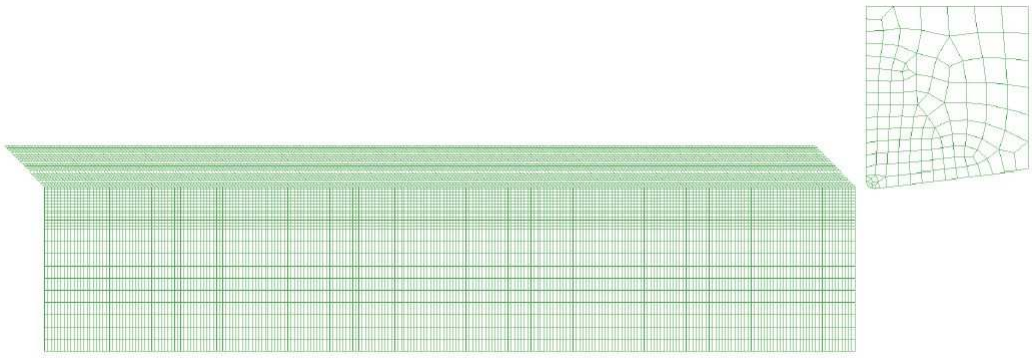

b)

Fig.1: High speed orthogonal machining configuration. After [6].

- Meshing

For the weak thermo-mechanical coupling, the workpiece is meshed with CPE4R 2D plane strain 4-node finite elements (reduced integration) and the tool with CPE3 2D plane strain 3-node finite elements and CPE4R 2D plane strain 4-node finite elements (reduced integration).

For the full thermo-mechanical coupling, the workpiece is meshed with CPE4RT 2D plane strain 4-node temperature-displacement coupled finite elements (reduced integration) and the tool with CPE3T 2D plane strain 3-node temperature-displacement coupled finite elements and CPE4RT 2D plane strain 4-node temperature-displacement coupled finite elements (reduced integration).

The meshed tool and workpiece before machining are shown in Fig.1b. A 45° chamfer is modelled in the workpiece right side to facilitate the machining beginning.

- Materials

The tool material is a Carbon-Boron-Nitride (CBN) alloy, assumed to be rigid in the simulation, with ρ=12700kg/m^3, C_p=234J/kg.K, Young's modulus E=500GPa and Poisson ratio ν=0.3.

The workpiece material is a Ti-6Al-4V titanium alloy, obeying Johnson-Cook constitutive law (implemented in Abaqus) with the constants in Table 1 where a is the thermal expansion coefficient. Different values of fracture strain ε_p^{crit} are assigned to each zone and different values of inelastic heat fraction β are considered for the parametric study.

- Initial conditions

The initial temperature T_0 for both the tool and the workpiece is 293 K.

- Boundary conditions

The lower side of the workpiece is clamped and the tool moves at a constant horizontal (x-axis in Fig.1a) negative velocity, the cutting speed, all along the machining process.

- Contact conditions

The contact between the tool and the workpiece is controlled by a Coulomb type friction law, coefficient of 0.5, with no heat transfer.

Table 1: Constants of the Ti-6Al-4V titanium alloy under consideration, after Molinari et al. (2013)

A (MPa)	B (MPa)	n	C	m	$\dot{\varepsilon}_0$ (1/s)
782	498	0.28	0.028	1.0	10^{-5}

k (W/mK)	C_p (J/kg.K)	a (μm/mK)	T_m	ρ (kg/m^3)	E (GPa)
7.2	560	9.2	1930	4420	114

4. Parametric study

Numerical simulations are conducted considering cutting speeds ranging from 3m/s to 350m/s. The cutting speed lowest value allows heat transfer whereas the highest one involves quasi-adiabatic conditions. According to Molinari et al. (2013) and Miguélez et al. (2013), the numerical model described in Sections 2 and 3 above is well able to reproduce the experimental results in terms of cutting force, thrust force and shear band spacing. It is now required to analyse the robustness of this model by testing its dependence on certain constants which are

usually chosen arbitrarily. Firstly, the interest of switching from full to weak thermo-mechanical coupling is explored. Then the influence of the critical plastic strain to failure ε_p^{crit} and inelastic heat fraction β on the chip morphology is studied.

4.1. Full vs Weak thermo-mechanical coupling

The interest of switching from full to weak thermo-mechanical coupling would be to gain in computational time. In addition, it seems reasonable to consider that as the cutting speed increases, the conditions are near adiabatic due to the limited characteristic time of the process. Here, the chip morphology obtained from the simulation of full and weak coupling are compared with some experimental observations obtained in Ye et al. (2013). In this section, the values of ε_{crit}^{p} for the zones A, B and C are assumed to be 6, 3 and 3 respectively and β equals 0.9 (most widely used value). It might seem paradoxical to assign a high value of fracture strain for the chip (zone A) and a low value for the substrate (zone B), but this favors the failure of the intermediate layer (zone B) elements located near the chip/layer (A/B) interface while avoiding a premature fragmentation of the chip.

A global view of the numerical simulation with fully coupled analysis at a cutting speed of 3m/s (180m/min) allowing heat transfer is shown in Fig.2 at a given time during the machining process. The elements in the intermediate layer get progressively deleted as the critical plastic strain ε_{crit}^{p} is reached while the tool cuts through the workpiece. The top zone forms the chip which when closely observed shows mild serration in this case.

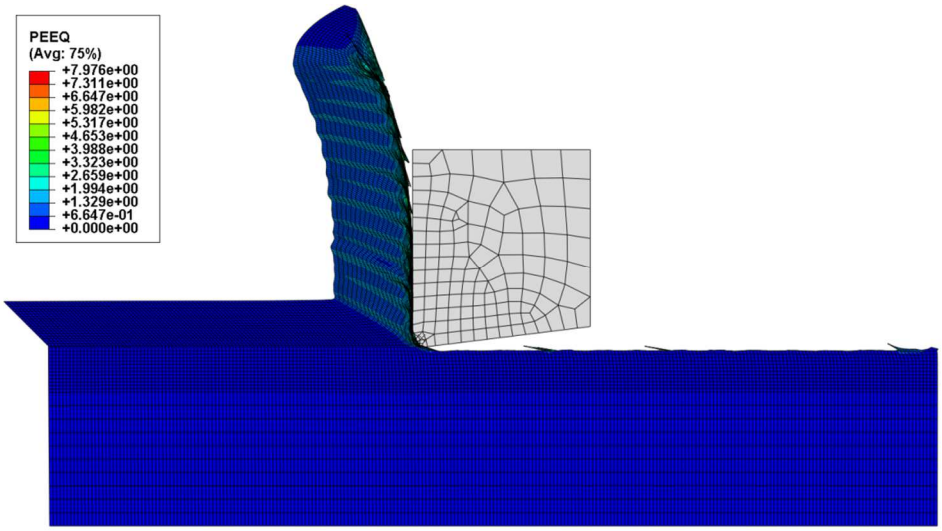

Fig.2: Global view of the fully coupled analysis of orthogonal machining at a cutting speed of 3m/s. Cumulated plastic strain ε_p (PEEQ) map.

The evolution of the chip formation is shown in Fig.3 for a fully coupled analysis at a cutting speed of 150m/s (9000m/min) corresponding to high-speed machining. This configuration exhibits serration without segmentation, i.e. preserving the chip cohesion.

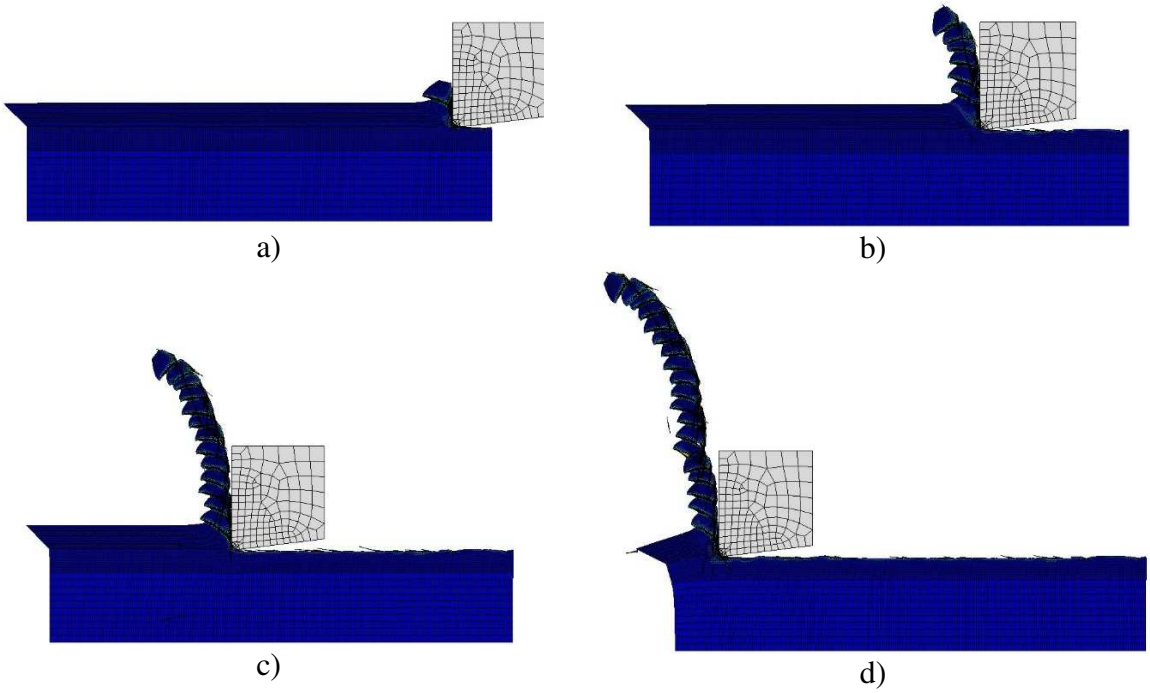

Fig.3: Global view of the fully coupled analysis of orthogonal machining at a cutting speed of 150m/s. Chip formation along the high-speed machining process.

Fully and weakly coupled analyses are conducted at cutting speeds of 5m/s (300m/min), corresponding to conventional machining, and 31.2m/s (1872m/min), corresponding to high-speed machining, in view of comparing the obtained chip morphologies with those observed experimentally in Ye et al. (2013). Heat transfers are expected to be allowed for the lowest cutting speed whereas adiabatic conditions are close to be reached for the highest one. Complementary fully and weakly coupled analyses are also conducted at a cutting speed of 350m/s (21000m/min), corresponding to ultra-high-speed machining according to Wang and co-authors' terminology, see Wang et al. (2015), and involving adiabatic conditions. Chip morphologies for the above-mentioned configurations are shown in Fig.4.

According to Fig.4a, for a low cutting velocity of 5m/s (300m/min) the microstructure evidences the role of shear banding in chip serration, see Fig.4a top. It is reminded that ASB is not explicitly accounted for in the numerical simulation. According to Fig.4a bottom, the full thermomechanical coupling produces numerical serrated chips close to the experiment whereas for the weak thermomechanical coupling the chip gets fragmented.

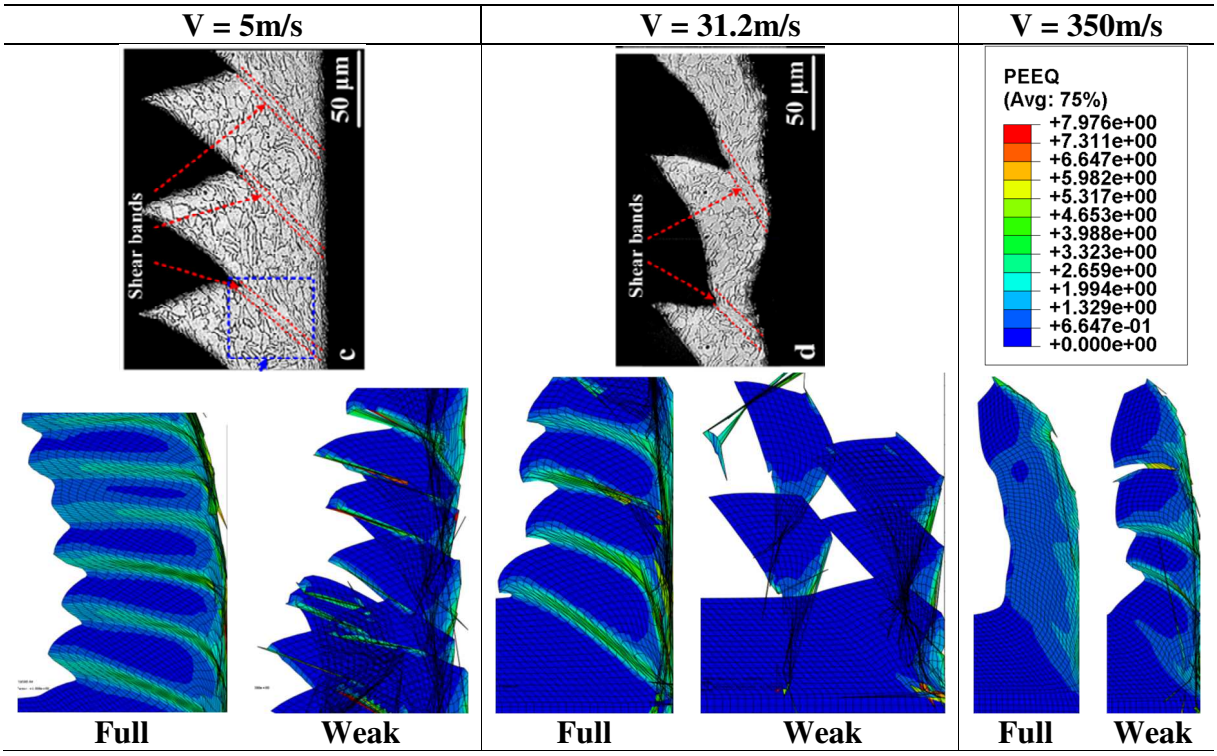

a) b) c)

Fig.4: Accumulated plastic strain ε_p map showing the chip morphology obtained from numerical simulation for full and weak coupling at cutting velocities of (a) V=5m/s (b) V=31.2m/s and (c) V=350m/s. Experimental chip micrograph after Ye et al. (2013).

According to Fig.4b, for the cutting velocity of 31.2 m/s (1872m/min) which falls in the category of high-speed machining (as a lower bound), the microstructure shows almost fragmented chips along the shear bands with a small portion remaining intact, see Fig.4b top. This experimental result lies in between of what is numerically simulated with fully and weakly coupled analyses, see Fig.4b bottom.

The very high ballistic-like cutting speed of 350m/s (21000m/min) in Fig.4c lacks of experimental results in literature. The simulation shows diffused high strain regions for the full coupling and shear localized almost fragmented chips for the weak coupling, see Fig.4c.

From these comments, one can conclude that, within a cutting speed range covering conventional and high-speed machining, passing from a fully to a weakly coupled analysis favors the chip segmentation. The experimental chip morphology lies in-between. At very high cutting speed, this trend inverts and the chip numerically obtained with the fully coupled analysis may even be continuous. This still needs to be experimentally confirmed, knowing that ASB is not explicitly taken into consideration in the numerical modeling.

4.2. Fracture criterion ε_{crit}^{p}

The more or less multi-dependent critical plastic strain to failure is usually chosen arbitrarily. Here the ε_{crit}^{p} of the different zones is given various values to see how much it affects the chip morphology. At first the ε_{crit}^{p} of zones A and C, i.e. the chip and base zone in Fig.1a, are kept constant with values of 6 and 3 respectively, whereas the ε_{crit}^{p} of zone B corresponding to the intermediate layer in Fig.1b is given values of 2, 3 and 4.

Results of the simulations conducted for a cutting speed of 3 m/s with a fully coupled analysis are shown in Fig.5 in terms of cumulated plastic strain ε_p (PEEQ) and temperature T (TEMP). It can be seen that $\varepsilon_{crit}^{p} = 2$ yields almost a continuous chip, $\varepsilon_{crit}^{p} = 3$ shows the initiation of the chip serration and $\varepsilon_{crit}^{p} = 4$ shows shear localization. Moreover, the number of plies at the surface of the chip is increasing and the shear band spacing is decreasing with the increasing value of ε_{crit}^{p}. Temperature T may locally reach values close to 1100K (827°C), viz. a temperature rise close to 627K.

In Fig.6, the ε_{crit}^{p} of the zone B is kept constant with the value 2 and its values for the zones A and C are varied equally, viz. 6, 8 and 10. The trend shows that increasing values of ε_{crit}^{p} renders more strain localized chips. Although this case does not exhibit much difference in the chip morphology, the previous case with the effect of the ε_{crit}^{p} of the intermediate layer is shown significant.

4.3. Inelastic heat fraction β

The other important quantity employed in high-speed machining models is the inelastic heat fraction β aimed at reproducing the plastic dissipation induced temperature rise, see eqs.(9-10). In literature, the arbitrary value usually taken for β is 0.9 by reference to the works by Taylor and Quinney (1934). In Longère and Dragon (2009), it has been shown that the inelastic heat fraction deduced from the irreversible thermodynamics based theoretical approach applied to the Johnson-Cook model is of the order of 0.3 (see Fig.8 in the cited article, simplified approach). A parametric study is accordingly carried out here to see how much the choice of the value of β is significant. Numerical simulations are conducted for $\beta = 0.3$, 0.6 and 0.9 and for both fully and weakly coupled cases.

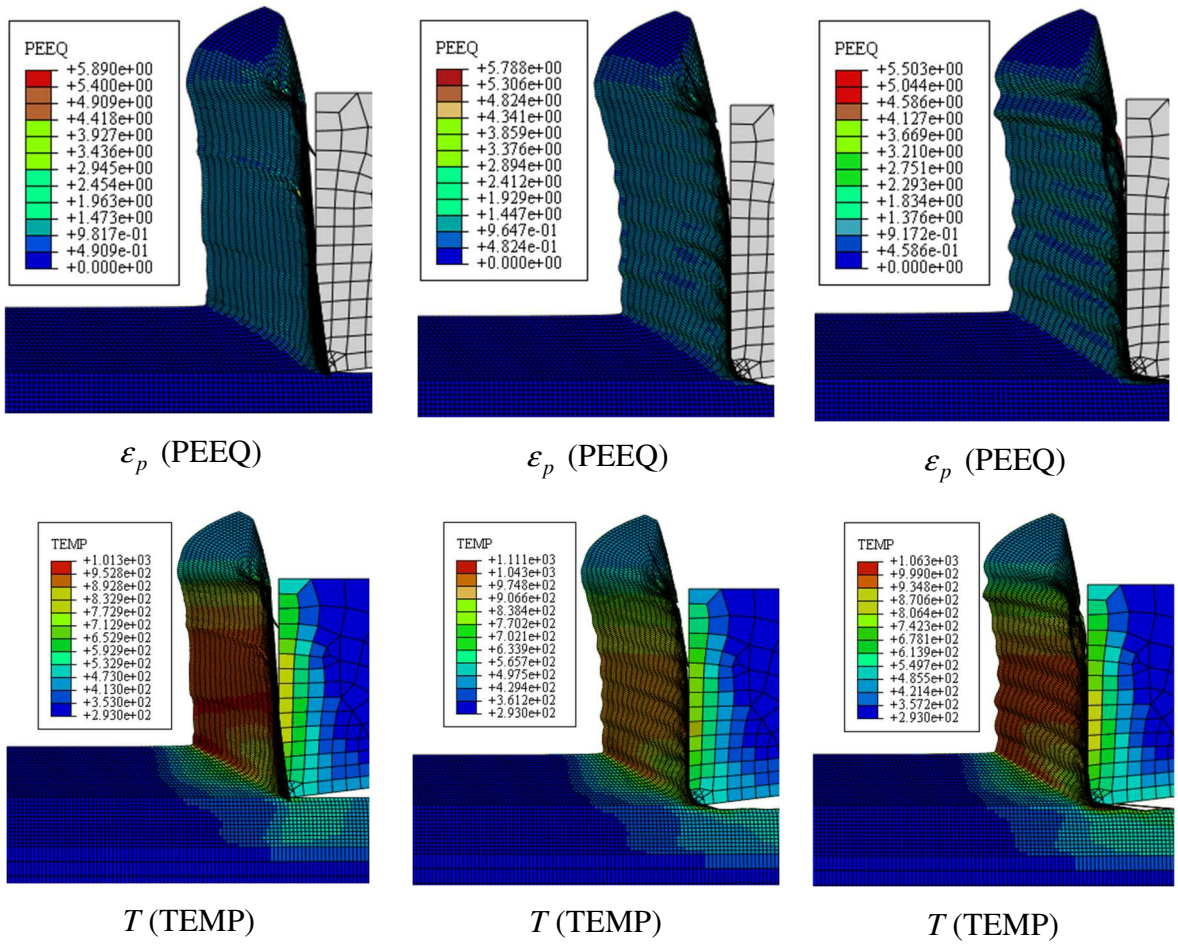

Fig.5: Cumulated plastic strain ε_p and temperature T maps showing the chip morphology for varying ε_{crit}^p of the zone B. Left: $\varepsilon_{crit}^p = 2$. Middle: $\varepsilon_{crit}^p = 3$. Right: $\varepsilon_{crit}^p = 4$. Fully coupled analysis. Cutting speed of 3 m/s. β=0.9.

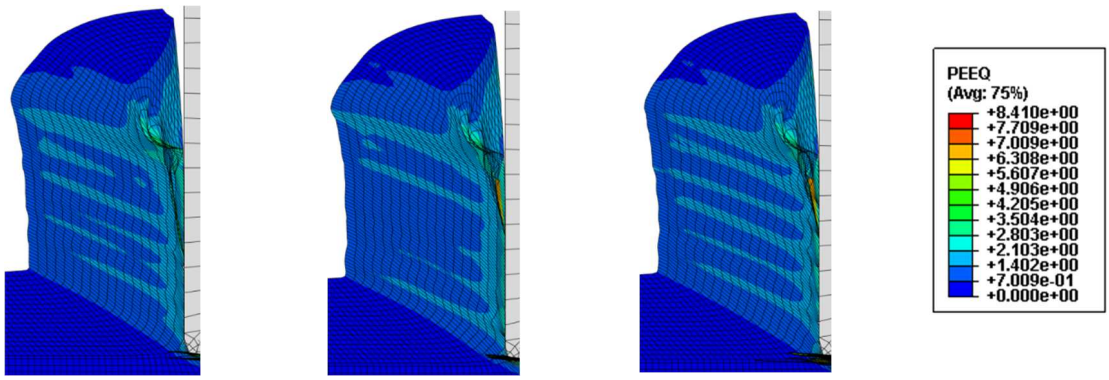

(a) (b) (c)

Fig.6: Cumulated plastic strain ε_p map showing the chip morphology for varying ε_{crit}^p of the zones A and C (a) $\varepsilon_{crit}^p = 6$, (b) $\varepsilon_{crit}^p = 8$, (c) $\varepsilon_{crit}^p = 10$. Fully coupled analysis. Cutting speed of 3 m/s. β=0.9.

The numerical results are displayed for some cases in Fig.7 in terms of cumulated plastic strain ε_p map for various cutting speeds and thermomechanical couplings. For $\beta = 0.3$ no shear bands are seen whatever the case. At the very high cutting speed of 350 m/s, diffused strain localization was observed for all the values of β in the fully coupled analyses. In all other cases, the general trend seen is that, with increasing value of β, i.e. more the proportion of plastic work converted to heat, more the chips show strain localization and chip segmentation. Other numerical results are displayed in Fig.8 in terms of temperature T map for the fully coupled case and at the cutting speed of 150m/s. It can be seen that the higher the value of β the more fragmented the chip. The maximum local temperature does not evolve much between $\beta = 0.3$ and $\beta = 0.6$ whereas a jump is observed for $\beta = 0.9$. The high values of local temperature, between 1540K and 1700K (1267°C and 1427°C), are above the experimental ones reported in Aboukshim et al. (2006). A difference of around 160K is observed between $\beta = 0.3$-0.6 and $\beta = 0.9$.

The shear band spacing vs β is plotted for full and weak couplings in Fig.9. The band spacing equaling zero in the graphs means that no shear bands were observed.

5. Discussion

According to the previous parametric study, temperature plays a major role in the serration and further segmentation of the chip. In the numerical simulation, irrespective of the constitutive model, the type of thermomechanical analysis (full vs weak) and the inelastic heat fraction β value (and possible evolution along the plastic deformation process) control the temperature rise and further thermal softening. The latter conditions the shear localization occurrence and then the serration formation. Yet, surprisingly, the individual and combined effects of these crucial parameters are rarely studied in the numerical works devoted to machining in general and high-speed machining in particular. Indeed, the coupled analysis type and the inelastic heat fraction value are generally arbitrarily chosen, without measuring the consequences of such choices, and the effort is rather put on refining the constitutive model and fracture criterion. However, the model and criterion coefficients are supposed to be previously calibrated via an experimental campaign including e.g. tension, compression and shear tests at various strain rates and temperatures, in the spirit of the V&V (verification and validation) procedure.

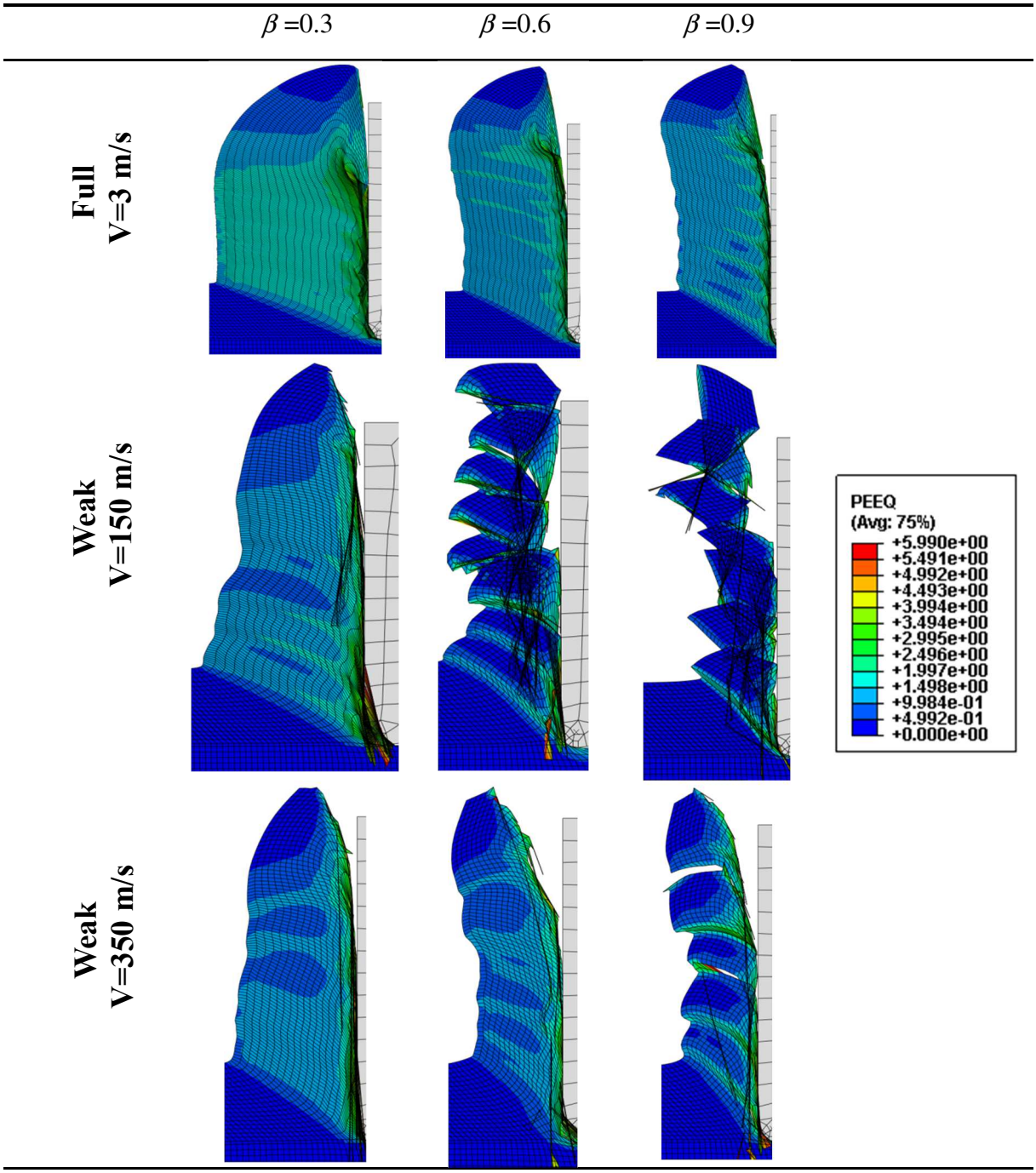

Fig.7: Cumulated plastic strain ε_p map showing the chip morphology for varying β and cases of thermo-mechanical coupling.

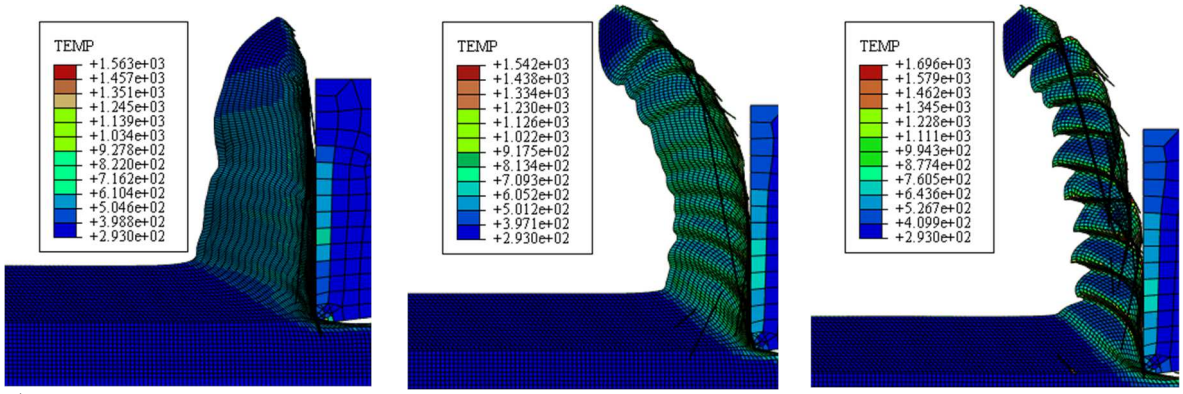

a) b) c)

Fig.8: Temperature T map showing the chip morphology for varying ε_{crit}^{p} of the zones A and C (a) $\beta = 0.3$, (b) $\beta = 0.6$, (c) $\beta = 0.9$. Fully coupled analysis. Cutting speed of 150 m/s.

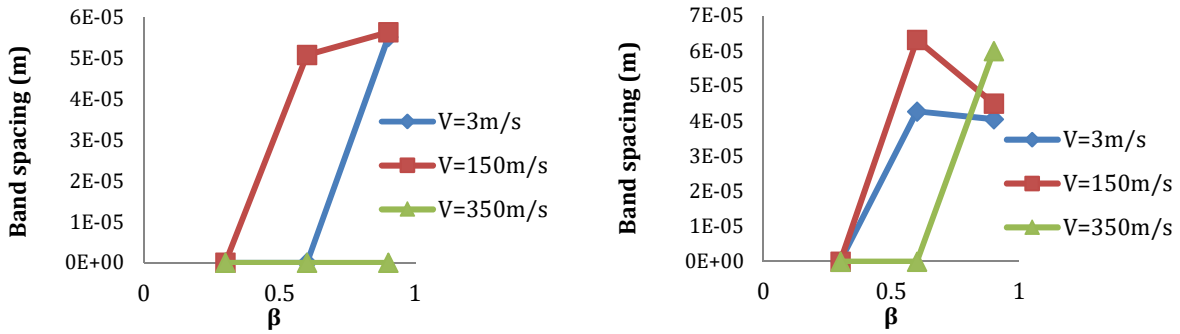

(a) (b)

Fig.9: Variation of shear banding spacing with β for (a) Full coupling (b) Weak coupling

5.1. Fully vs weakly coupled thermomechanical analysis

For low-to-moderate high-strain rate loading involved during conventional machining, discrepancies must appear in the numerical results between fully and weakly coupled thermo-mechanical analyses since thermal conditions are neither isothermal nor adiabatic. Now, under high-strain rate loading involved during high-speed and ultra-high-speed machining, conditions are (quasi-) adiabatic and both fully and weakly coupled thermo-mechanical analyses are accordingly expected to provide the same results, to within a few slight discrepancies. Yet, this is clearly not the case since results strongly depend on the coupled analysis type, see Fig.4.b.

It is well-known that numerical results obtained from standard finite element analysis suffer from a pathological mesh size and orientation dependence in the softening regime. This dependence results in a strain localization concentrated within a band of a single finite element-width, which is purely numerical and not physical, see Longère (2018), hence the need for regularization. It has been shown that viscosity and thermal diffusion both contribute to regularizing the numerical results, see e.g. Needleman (1988) and Areias and Belytschko

(2007). According to the above parametric study the regularizing effect of viscoplasticity is clearly insufficient, see Fig.4a.b (Weak). The regularizing effect of thermal diffusion seems more efficient, with a strain localization bandwidth covering several finite elements, see Fig.4a.b. (Full) and Fig.6. The fully coupled thermo-mechanical analyses should accordingly be preferred.

The case of ultra-high-speed machining in Fig.4.c still needs to be confirmed by experimental results before being discussed.

5.2. Self-heating and inelastic heat fraction

The inelastic heat fraction is the key-parameter for triggering the thermal softening-induced strain localization leading to serration and further fragmentation. However, although Xu et al. (2020) and Liu et al. (2020) insist on the importance of heat generation, they surprisingly consider only chip/tool friction induced heating and not material self-heating. Similarly, in its review on constitutive modelling devoted to high-speed machining, Melkote et al. (2017) do not evoke at all self-heating nor the inelastic heat fraction. As previously mentioned, the inelastic heat fraction has been experimentally shown to evolve along the plastic deformation process, see Mason et al. (1994) and Rosakis et al. (2000). Yet, in most numerical simulations devoted to high-speed machining, it is still considered constant, with values unrealistically high (0.9-1), see e.g. Zhang et al. (2015), Wang et al. (2016) and Ye et al. (2013), leading to overestimating the temperature rise and accordingly rending premature the serration and fragmentation, see Fig.7. Commercial computation codes have probably some responsibility in this coarse simplification in the sense that the inelastic heat fraction is an input data. However, the inelastic heat fraction should result from the thermodynamic framework consistently with the adopted constitutive model, see e.g. Ruiz des Sotto et al. (2020), and not be a priori defined. This supposes a physics-motivated constitutive model able to account for the underlying mechanisms playing a role in the thermo-mechanical coupling and not a purely empirical engineering-oriented constitutive model merely aimed at fitting stress-strain responses. Consequently, the designer cannot be content with the constitutive models implemented by default in commercial computation codes and should use/implement user defined material subroutines wherein the material heat source consistently derives from the constitutive model, see Rosakis et al. (2000) and Longère and Dragon (2008,2009).

5.3. From strain localization to failure

The reader can refer to Longère (2018) for details on the concept of small/large-scale postulate cited in the following.

Most numerical simulations involving strain localization like ASB are conducted in the context of the small-scale postulate, that means the bandwidth is expected to cover several finite elements, implying that the bandwidth is greater than the finite element characteristic length. This is generally the case within the step of weakly heterogeneous deformation (which precedes the strain localization) where a smooth strain gradient is reproduced. Now, as previously mentioned, the intensification of the softening regime leads to the formation of highly deformed bands (resulting from numerical instability and not from material instability) of a single finite element-width supposed to reproduce the step of strongly heterogeneous deformation (corresponding to strain localization). As a consequence, the chip morphology induced by the finite element failure, either conditioned by a constant fracture strain, as done in the present work, or by a multi-dependent fracture strain, as done in e.g. Mabrouki et al. (2008) and Zhang et al. (2015), actually results from a numerical instability and not from a material instability. It has been shown in section 5.1 that thermal diffusion has a partial but often insufficient regularizing effect.

Controlling the strain localization formation (initiation and evolution) may be achieved by switching from the small-scale postulate to the large-scale postulate. According to the latter, from a two-dimensional viewpoint, the band is embedded within the finite element, that means the bandwidth is smaller than the finite element size. For example, the strain localization band may be considered as a form of induced plastic anisotropy whose material and kinematic consequences are described at the constitutive model level. This is the approach adopted in Longère et al. (2009) for the strain localization (ASB) and Lois Dorothy et al. (2019) that additionally accounts for micro-voiding induced damage and failure. The model has been implemented as a user material subroutine in LS-DYNA and has proven efficient for some high-strain rate loading cases. The strain localization band may also be considered as a proper entity whose kinematic consequences are reproduced at the finite element level. This is the approach adopted in two-dimension in Wolf et al. (2018) and in three-dimension in Nikolakopoulos et al. (2021) wherein the strain localization band is viewed as a cohesive strong discontinuity leading progressively to the formation of a crack. This numerical approach has been implemented following the eXtended Finite Element Method (XFEM) as a user element subroutine in

Abaqus-Std. It has proven efficient for some low-strain rate loading cases and still needs to be extended to transient dynamics.

5. Conclusion

The parametric study conducted in the present paper demonstrates that the chip morphology during high speed machining is strongly influenced by (i) the level of thermo-mechanical coupling (full vs weak), (ii) the method for evaluating the temperature rise (via the inelastic heat fraction β often assumed to be constant) and (iii) the value of the failure strain. Two cases of thermo-mechanical coupled analyses are explored – strong coupling (with heat conduction) and weak coupling (adiabatic condition). At low-to-high cutting speeds, the strongly coupled analysis renders accurate outcome and at ultra-high cutting speeds it is possible that the weakly coupled analysis is more accurate although it needs to be backed by experimental evidence.
In order to rend the numerical results objective with respect to the meshing, it is suggested to switch from the small-scale postulate to the large-scale postulate.

References

Abukhshim N.A., Mativenga P.T., Sheikh M.A., 2006, Heat generation and temperature prediction in metal cutting: A review and implications for high speed machining, Int. J. Machine Tools & Manuf., 46, 782–800

Areias P.M.A., Belytschko T., 2007, Two-scale method for shear bands: Thermal effects and variable bandwidth, Int. J. Numer. Meth. Eng; 72:658–696

Bai Y. L. and Dodd B., Adiabatic shear localization. Pergamon Press, Oxford., 1992

Bao Y., Wierzbicki T., 2004, On fracture locus in the equivalent strain and stress triaxiality space, Int. J. Mech. Sci., 46, pp.81-98

Calamaz M., Coupard D., and Girot F., 2008, A new material model for 2D numerical simulation of serrated chip formation when machining titanium alloy Ti – 6Al – 4V, Int. J. Mach. Tools Manuf., vol. 48, pp. 275–288

Chen X., Tang J., Ding H., Liu A., 2021, A new geometric model of serrated chip formation in high-speed machining, J. Manuf. Proc., 62, 632–645

Chowdhury M.S.I., Bose B., Yamamoto K., Shuster L.S., Paiva J., Fox-Rabinovich G.S., Veldhuis S.C., 2020, Wear performance investigation of PVD coated and uncoated carbide tools during high-speed machining of TiAl6V4 aerospace alloy, Wear, 446-447, 203168

Fu H., Zhou X., Wu B., Qian L., Yang X.S., 2021, Atomic-scale dissecting the formation mechanism of gradient nanostructured layer on Mg alloy processed by a novel high-speed machining technique, J. Mater. Sci. & Tech., 82, 227–238

Gentel A., Hoffmeiste H.-W., 2001, Chip Formation in Machining Ti6A14V at Extremely High Cutting Speeds, CIRP Annals, 50-1, pp.49-52

Hemmati A., DePaiva J.M., Veldhuis S.C., 2022, An in-depth investigation of the machining performance of Ti1-Xalxn PVD coatings during high-speed machining of 316 stainless steel, J. Manuf. Proc., 75, pp.903–918

Ivester R, Whitenton E, Deshayes L (2005) Comparison of Measurements and Simulation for Machining of Aluminum. Transactions of the North American Manufacturing Research Institution of SME 33:429–436.

Johnson G.R., Cook W.H., 1983, A constitutive model and data for metals subjected to large strains, high strain rates and high temperatures, in Proceedings of the Seventh International Symposium on Ballistics, The Hague, The Netherlands, pp.541-547.

Johnson G.R., Cook W.H., 1985, Fracture characteristics of three metals subjected to various strains, strain rates, temperatures and pressures. Eng. Fract. Mech., 21-1, pp.31–48.

Larbi S., Djebali S., Bilek A., 2015, Study of High Speed Machining by Using Split Hopkinson Pressure Bar, Proc. Eng., 114, 314 – 321

Lemaître, J. 1985, A continuous damage mechanics model for ductile fracture, J. Eng. Mat. Tech., ASME, 107, pp.83-89

Liu H., Zhang J., Xu B., Xu X., Zhao W., 2020, Prediction of microstructure gradient distribution in machined surface induced by high speed machining through a coupled FE and CA approach, Mater. Design, 196, 109133

Lois Dorothy H., Longère P., 2019, Unified modelling of adiabatic shear banding and subsequent micro-voiding driven dynamic failure of viscoplastic solids, Int. J. Impact Eng., 132, 103322

Longère P., 2018, Adiabatic shear banding assisted dynamic failure: Some modeling issues, Mech. Mater., vol. 116, pp. 49–66, 2018.

Longère P., Dragon A., 2008, Evaluation of the inelastic heat fraction in the context of microstructure-supported dynamic plasticity modelling, Int. J. Impact Eng. 35 992–999

Longère P., Dragon A., 2009, Inelastic heat fraction evaluation for engineering problems involving dynamic plastic localization phenomena, J. Mech. Mat. Struct., 4-2, 319-349

Longère P., Dragon A., 2013, Description of shear failure in ductile metals via back stress concept linked to damage-microporosity softening, Eng. Fract. Mech. 98 92–108

Longère P., Dragon A., Deprince X., 2009, Numerical study of impact penetration shearing employing finite strain viscoplasticity model incorporating adiabatic shear banding, J. Eng. Mat. Tech., ASME, 131, pp.011105.1-14

Mabrouki T., Girardin F., Asad M., Rigal J.F., 2008, Numerical and experimental study of dry cutting for an aeronautic aluminium alloy (A2024-T351), Int. J. Machine Tools & Manuf., 48, 1187– 1197

Mason J.J., Rosakis A.J., Ravichandran G., 1994, On the strain and strain rate dependence of the fraction of plastic work converted to heat: an experimental study using high speed infrared detectors and the Kolsky bar, Mech. Mat., 17, 135-145

Melkote S.N., Grzesik W., Outeiro J., Rech J., Schulze V., Attia H., Arrazola P.J., M'Saoubi R., Saldana C., 2017, Advances in material and friction data for modelling of metal machining, CIRP Annals – Manuf. Tech., 66, 731–754

Molinari A., Musquar C., Sutter G., 2002, Adiabatic shear banding in high speed machining of Ti–6Al–4V: experiments and modeling, Int. J. Plast., 18, pp.443–459

Moufki A., Devillez A., Dudzinski D., Molinari A., 2004, Thermomechanical modelling of oblique cutting and experimental validation, 2004, Int. J. Machine Tools & Manuf., 44, pp.971–989

Moufki A., Molinari A., Dudzinski D., 1998, Modelling of orthogonal cutting with a temperature dependent friction law, 1998, J. Mech. Phys. Solids, 35-9, pp.1092-1027

Needleman A., 1988, Material rate dependence and mesh sensitivity in localization problems, Computer Methods Appl. Mech. Eng., 67, 69-85

Nikolakopoulos K., Crété J.P., Longère, P., 2021, Progressive failure of ductile metals: Description via a three-dimensional coupled CZM–XFEM based approach, Eng. Fract. Mech., 243, 107498

Rosakis P., Rosakis A.J., Ravichandran G., Hodowany J., 2000, A thermodynamic internal variable model for the partition of plastic work into heat and stored energy in metals, J. Mech. Phys. Solids 48 581-607

Ruiz de Sotto M., Doquet V., Longère P., Papasidero J., 2021, Anisotropic, rate-dependent ductile fracture of Ti-6Al-4V alloy, Int. J. Dam. Mech.

Ruiz de Sotto M., Longère, Doquet V., Papasidero J., 2020, A constitutive model for a rate and temperature-dependent, plastically anisotropic titanium alloy, Int. J. Plast., 134, 102777

Seo S., Min O., and Yang H., 2005, Constitutive equation for Ti–6Al–4V at high temperatures measured using the SHPB technique," vol. 31, pp. 735–754

Sutter G., Molinari A., Faure L., Klepaczko J.R., Dudzinski D., An Experimental Study of High Speed Orthogonal Cutting, J. Manuf. Sci. Eng., ASME, 120, pp.169-172

Taylor G.I, Quinney H., 1934, The latent energy remaining in a metal after cold working, Proc. Roy. Soc., A413, pp.307-326

Umbrello D., 2008, Finite element simulation of conventional and high speed machining of Ti6Al4V alloy, 196, pp.79–87

Wang B., Liu Z., 2016, Evaluation on fracture locus of serrated chip generation with stress triaxiality in high speed machining of Ti6Al4V, Mater. Design, 98, 68–78

Wang B., Liu Z., Su G., Song Q., Ai X., 2015, Investigations of critical cutting speed and ductile-to-brittle transition mechanism for workpiece material in ultra-high speed machining, Int. J. Mech. Sci., 104, 44–59

Wolf J., Longère P., Cadou J.M., Crété, 2018, Numerical modeling of strain localization in engineering ductile materials combining cohesive models and X-FEM, Int J Mech Mater Des (2018) 14:177–193

Xi X., Bermingham M., Wang G., Dargusch M., 2014, SPH/FE modeling of cutting force and chip formation during thermally assisted machining of Ti6Al4V alloy, Comput. Mater. Sci., 84, 188–197

Xu X., Zhang J., Outeiro J., Xu B., Zhao W., 2020, Multiscale simulation of grain refinement induced by dynamic recrystallization of Ti6Al4V alloy during high speed machining, J. Mater. Proc. Tech., 286, 116834

Ye G. G., Xue S. F., Jiang M. Q., Tong X. H., and Dai L. H., 2013, Modeling periodic adiabatic shear band evolution during high speed machining Ti-6Al-4V alloy, Int. J. Plast., 40, pp. 39–55

Zhang Y., Outeiro J.C., Mabrouki T., 2015, On the selection of Johnson-Cook constitutive model parameters for Ti-6Al-4V using three types of numerical models of orthogonal cutting, Proc. CIRP 31, 112 – 117

Advances in Materials and Processing Technologies Ref.: Ms. No. TMPT-2019-0041

Response to reviewers

Adiabatic Shear Band assisted chip serration in High Speed Machining: Some Modelling Issues

Is the title of the article adequately represent the content of the article ? Reviewer 1: No:

Is the title of the article adequately represent the content of the article ? Reviewer 2: No:

Are there, an Abstract, List of Key Words and Conclusions present in the article ? Reviewer 2: Yes: Yes, but the conclusions could be written more directly

Are the references cited in either Scientific (by number only) or Cambridge style (by author name and year of publication)? (Both systems are acceptable but not mixed System). Reviewer 2: Yes, but the authors could have used newer references

The authors have read with much attention the comments raised by the two Reviewers and are appreciative of the advices offered. According to the Reviewers' recommendations, the authors have attempted to improve the manuscript by changing the title, enhancing the Introduction, bringing many complements for a better understanding, and completing the list of references with recent ones. The authors hope that this revised version of the paper meets the Reviewers' and Editor's expectations.

Reviewer #1:

1. The title of the paper recommended to be changed to " Effect of xxxxx model on the adiabatic band formation of Ti-6Al-4V alloy".

In order to better match the content of the paper, the title has been changed as follows:

A parametric numerical study of ASB-assisted chip formation in high-speed machining of Ti-6Al-4V

Need to mention the exact modelling used for the simulation.

As mentioned in the revised version, the tool material is a Carbon-Boron-Nitride (CBN) alloy, assumed to be rigid and the workpiece material is a Ti-6Al-4V titanium alloy, obeying Johnson-Cook constitutive law (implemented in Abaqus) with the constants in Table 1

The geometry, the meshing, and the initial, boundary and contact conditions have been detailed.

2. In the methodology, it is recommended to present the exact figure from the Abaqus. For example the images that presenting the mesh of workpiece and the cutting tool.

The meshed tool and workpiece before machining are shown in Fig.1b in the revised version of the manuscript.

3. In the methodology, present the images that show the progressive of the chip formation from time=0 to time 3 m/s.

The evolution of the chip formation is shown in Fig.3 in the revised version of the manuscript for a fully coupled analysis at a cutting speed of 150m/s (9000m/min) corresponding to high-speed machining.

4. Kindly state whether the authors use user subroutine of not.

As above mentioned, the Johnson-Cook constitutive model as implemented by default in Abaqus has been used to reproduce the work piece material behaviour.

5. List of references are very limited and not up to date.

The number of references has been multiplied by more than 2, passing from 19 in the original paper to 44 in the revised paper, with 11 published between 2010 and 2019 and 9 published between 2020 and today.

Reviewer #2:

1. The work studies the use of HSM, however, speeds of 3m/s used in the simulations, even for titanium are far from being HSM. The authors could have focused only on HSM speeds and studied small variations. In this sense, the title is not entirely in accordance with the content of the work;

In the present study, lower cutting speeds are also explored in order to test the accuracy of the numerical model in predicting the chip morphology. The higher cutting speeds exhibit the formation of adiabatic shear bands as expected.

2. The review is small, has few references. The references are mostly old.

The review in the Introduction and in the other sections as well as the list of references have been significantly completed, see answer to Reviewer#1' Question 5.

3. What is the practical contribution of work to the process? What can the study bring in practical terms to the HSM process?

As mentioned in The Introduction, the aim is to evidence some issues/limitations in the numerical simulation of high-speed machining and provide the designer with elements for parameterizing his/her optimization process. For that purpose, the present engineering-oriented study focuses on the influence of the way the thermo-mechanical coupling and material failure are accounted for. More precisely, starting from models available by default in the computation code, comparisons will be made between full and weak thermo-mechanical coupling, and the influence of the fracture strain and inelastic heat fraction values will be studied.

In Section 5. Discussion, the authors give recommendations to increase the robustness of the numerical modeling.

4. I believe that the authors can work a little more on the introduction to illustrate the importance of the study, with practical results designed by other authors and direct the work towards this purpose.

Thanks to a more detailed review relying upon recent works, the Introduction has been thoroughly enhanced.